Received: 30 June 2021 | Revised: 18 November 2021 | Accepted: 21 November 2021

DOI: 10.1111/gcb.16017

Global Change Biology WILEY

PRIMARY RESEARCH ARTICLE

Tropical tall forests are more sensitive and vulnerable to drought than short forests

Liyang Liu[1,2,3] | Xiuzhi Chen[1] | Philippe Ciais[3] | Wenping Yuan[1] | Fabienne Maignan[3] | Jin Wu[4] | Shilong Piao[5] | Ying-Ping Wang[6] | Jean-Pierre Wigneron[7] | Lei Fan[8] | Pierre Gentine[9] | Xueqin Yang[1,2] | Fanxi Gong[1] | Hui Liu[10] | Chen Wang[10] | Xuli Tang[10] | Hui Yang[3] | Qing Ye[10] | Bin He[11] | Jiali Shang[12] | Yongxian Su[2]

[1]Guangdong Province Key Laboratory for Climate Change and Natural Disaster Studies, School of Atmospheric Sciences, Sun Yat-sen University & Southern Marine Science and Engineering Guangdong Laboratory (Zhuhai), Zhuhai, China

[2]Key Lab of Guangdong for Utilization of Remote Sensing and Geographical Information System, Guangdong Open Laboratory of Geospatial Information Technology and Application, Guangzhou Institute of Geography, Guangdong Academy of Sciences, Guangzhou, China

[3]Laboratoire des Sciences du Climat et de l'Environnement, IPSL, CEA-CNRS-UVSQ, Université Paris-Saclay, Gif sur Yvette, France

[4]School of Biological Sciences, The University of Hong Kong, Pokfulam, Hong Kong

[5]Sino-French Institute for Earth System Science, College of Urban and Environmental Sciences, Peking University, Beijing, China

[6]CSIRO Oceans and Atmosphere, Aspendale, Victoria, Australia

[7]ISPA, UMR 1391, INRA Nouvelle-Aquitaine, Bordeaux Villenave d'Ornon, France

[8]Chongqing Jinfo Mountain Karst Ecosystem National Observation and Research Station, School of Geographical Sciences, Southwest University, Chongqing, China

[9]Department of Earth & Environmental Engineering, Columbia University, New York, New York, USA

[10]South China Botanical Garden, Chinese Academy of Sciences, Guangzhou, China

[11]State Key Laboratory of Earth Surface Processes and Resource Ecology, College of Global Change and Earth System Science, Beijing Normal University, Beijing, China

[12]Ottawa Research and Development Centre, Agriculture and Agri-Food Canada, Ottawa, Ontario, Canada

Correspondence
Xiuzhi Chen, Guangdong Province Key Laboratory for Climate Change and Natural Disaster Studies, School of Atmospheric Sciences, Sun Yat-sen University & Southern Marine Science and Engineering Guangdong Laboratory (Zhuhai), Zhuhai 519082, China.
Email: chenxzh73@mail.sysu.edu.cn

Funding information
National Natural Science Foundation of China, Grant/Award Number: 31971458 and 41971275; Guangdong Major Project of Basic and Applied Basic Research, Grant/Award Number: 2020B0301030004; ECOPROPHET PROJECT, Grant/Award Number: SR/00/334; Special high-level plan project of Guangdong Province, Grant/Award Number: 2016TQ03Z354

Abstract

Our limited understanding of the impacts of drought on tropical forests significantly impedes our ability in accurately predicting the impacts of climate change on this biome. Here, we investigated the impact of drought on the dynamics of forest canopies with different heights using time-series records of remotely sensed Ku-band vegetation optical depth (Ku-VOD), a proxy of top-canopy foliar mass and water content, and separated the signal of Ku-VOD changes into drought-induced reductions and subsequent non-drought gains. Both drought-induced reductions and non-drought increases in Ku-VOD varied significantly with canopy height. Taller tropical forests experienced greater relative Ku-VOD reductions during drought and larger non-drought increases than shorter forests, but the net effect of drought was more negative in the taller forests. Meta-analysis of in situ hydraulic traits supports the hypothesis that taller tropical forests are more vulnerable to drought stress due to smaller xylem-transport safety margins. Additionally, Ku-VOD of taller forests showed larger reductions due to increased atmospheric dryness, as assessed by vapor pressure deficit,

and showed larger gains in response to enhanced water supply than shorter forests. Including the height-dependent variation of hydraulic transport in ecosystem models will improve the simulated response of tropical forests to drought.

KEYWORDS
canopy dynamics, canopy height, drought, microwave remote sensing, tropical forests, vegetation optical depth

1 | INTRODUCTION

Drought impairs canopy photosynthesis and increases tree mortality, ultimately producing dead woods that emit CO_2 into the atmosphere for decades (Baccini et al., 2017; Fan et al., 2019; Hérault et al., 2010; Lewis et al., 2011; Liu et al., 2017; Malhi & Grace, 2000; Phillips et al., 2009; Wang et al., 2014; Yang, Ciais, et al., 2021). Tropical forests first close stomata and shed leaves to reduce transpirational water loss under drought conditions (Aguadé et al., 2015; Kono et al., 2019; Yazaki et al., 2015), and even experienced high mortality rates during prolonged droughts (da Costa et al., 2010; Phillips et al., 2009), with some regions showing lagged mortality (Yang et al., 2018). The inability of forests to completely recover from severe drought might lead to long-term forest biomass loss (Verbesselt et al., 2016). In contrast, some tropical forests, such as those in the Amazon region, were observed to sustain steady canopy growth and even increase net primary productivity during drought (Doughty et al., 2015). These seemingly conflicting observations highlight our limited understanding of the impact of drought on tropical forests.

The hydraulic failure hypothesis is one of the main hypotheses proposed to explain the impact of droughts on tropical forests (Kono et al., 2019). This hypothesis predicts that substantial and irreversible embolism in response to drought stress reduces photosynthesis, potentially leading to mortality due to cavitation events in the rhizosphere and xylem vessels (Kono et al., 2019; Rowland et al., 2015; Sperry et al., 2002; Tyree & Sperry, 1989). Canopy height (Hc) is an important trait that influences xylem water transport and photosynthesis (Brando, 2018; Gentine et al., 2016; Giardina et al., 2018). Some studies suggested that taller trees were more vulnerable to drought because of a higher risk of hydraulic failure associated with greater height (Barros et al., 2019; Liu et al., 2019; Mencuccini et al., 2005; Rowland et al., 2015). Experimental drought studies at two Amazonian tropical forest sites found that large and tall trees showed a greater risk of hydraulic deterioration than short trees, and showed high rates of mortality several years after partial rain exclusion, yet with small changes in net primary production at the ecosystem level because of compensatory growth from shorter individuals (Nepstad et al., 2007; Rowland et al., 2015). Conversely, several studies showed that taller trees were more resistant to drought (Brando, 2018) because they had deeper roots to access water from deeper soil (Giardina et al., 2018) and higher water use efficiency than shorter trees (Brienen et al., 2017). However, this viewpoint has been challenged by field observations showing no obvious relation between tree height and the rooting zone soil depth (Stahl et al., 2013). Therefore, the influence of tree height on the response of tropical forests to drought and subsequent non-drought growth remains controversial.

The main objective of this study was to investigate the drought-induced canopy dynamics of tropical forests with different canopy heights. We used a monthly satellite-based Ku-band microwave vegetation optical depth (VOD) product (Ku-VOD; Moesinger et al., 2020) as a proxy of foliage mass and water content of the forest upper canopy (Frolking et al., 2012; Guan et a., 2013; Saatchi et al., 2013) which is closely related to the top-canopy (TOC) leaf area index (LAI; method: Evaluation of the sensitivity of Ku-VOD to TOC LAI), and two LIDAR Hc datasets (Hc_{Simard} from Simard et al., 2011 and Hc_{GEDI} from Potapov et al., 2021; Table S1) to investigate whether taller tropical forests are more resilient than shorter ones in response to drought across three tropical continental regions (America (Amazon region), Africa, and Asia) from 1988 to 2015 (Table S2). Additionally, we discussed the potential strategies of plant hydraulics to explain drought-induced canopy dynamics in tropical forests with different canopy heights based on in situ eco-physiological observations.

2 | METHODS

2.1 | Method summary

To define drought, including both moderate and severe drought (Cook et al., 2014), we used an integrated drought criterion based on the Palmer drought severity index (PDSI; Abatzoglou et al., 2018; Palmer, 1965; Wang et al., 2014; Zhao & Running, 2010), the standardized precipitation evapotranspiration index (SPEI, with 6 months; Vicente-Serrano, Beguería, & López-Moreno, 2010; Vicente-Serrano, Beguería, López-Moreno, Angulo, et al., 2010), and cumulative water deficit (CWD; Aragão et al., 2007; Lewis et al., 2011; Malhi et al., 2009; Saatchi et al., 2013). Accordingly, a pixel is considered to experience drought when at least two of the corresponding monthly anomalies of the above three indices (PDSI, SPEI, and CWD) in a given month fall one standard deviation below the mean of the 1988–2015 time series. Then, we defined a year as a drought year (red circles, Figure S1) if the yearly regional percentage of forested drought pixels (hereafter denoted $Drought_{fraction}$) was above 20% ($Drought_{fraction}$ peaks), and as a non-drought year (blue circles, Figure S1) when $Drought_{fraction}$ reached a minimum

value between two corresponding drought years, for the Amazon, Africa, and Asia, respectively (Methods: Categorizing drought and non-drought years). For each pixel, we calculated the drought-induced Ku-VOD loss (ΔKu-VOD$_{drought}$) per drought year using the Ku-VOD during the drought period minus the Ku-VOD during the non-drought period (Figure S2, Methods). In turn, the canopy gain (ΔKu-VOD$_{non\text{-}drought}$) was calculated as the difference between Ku-VOD during the following non-drought year and the Ku-VOD during a current drought year (Figure S2, Methods). We used these paired quantities for each drought year and subsequent non-drought year to investigate whether the sensitivity of tropical forests to drought was significantly dependent on Hc.

2.2 | Study area

We focused on tropical broadleaved evergreen forests based on the MODIS land cover map (MCD12C1, 0.05° resolution; Sulla-Menashe & Friedl, 2018) and tree cover map (25 m resolution; Hansen et al., 2013). Thus, based on the land cover map, we extracted pixels corresponding to tropical evergreen broadleaved forests (EBF) in the pantropical, region at a spatial resolution of 0.05°, from 2001 to 2016, according to the classification in the International Geosphere-Biosphere Program (IGBP), and removed any pixels whose land-use type changed during this period. Then, we established a 0.5° × 0.5° grid for intact tropical areas and labeled EBF-dominated pixels, in which more than 50% of 0.05° pixels were tropical EBFs, and for each 0.5° pixel, we calculated the percentage of the 25 m pixels with forest coverage lower than 80% or affected by deforestation, using the Hansen tree deforestation maps (Hansen et al., 2013) from 2000 to 2016 (25 m resolution). Any 0.5° pixels with forest coverage <80% or deforestation higher than 20% were removed (Figure S3).

2.3 | Categorizing drought and non-drought years

The Palmer drought severity index (PDSI; Abatzoglou et al., 2018; Dai, 2013; Mera et al., 2018; Wang et al., 2014; Zhao & Running, 2010), the SPEI (with a 6-month scale; Vicente-Serrano, Beguería, & López-Moreno, 2010; Vicente-Serrano, Beguería, López-Moreno, Angulo, et al., 2010), and cumulative water deficit (CWD; Aragão et al., 2007; Lewis et al., 2011; Malhi et al., 2009; Saatchi et al., 2013; Supplementary Information) have been widely applied to detect forest drought across the tropical regions. However, the values of each drought index without anomalies vary significantly among pixels, whereby, it is difficult to set a consistent threshold for defining a drought. Thus, generally, one standard deviation of the drought index is used to indicate moderate or even more severe droughts (Cook et al., 2014). Therefore, we calculated the pixel-based $X_{anomaly}$ (i.e., the standardized anomaly of each drought index, X represents PDSI, SPEI, and CWD, respectively, in Equation 1) for each month, from 1988 to 2015. Then, we used three parameters to define a drought: (1) the PDSI standard deviation ≤−1 (PDSI$_{anomaly}$ ≤ −1), (2) SPEI standard deviation ≤ −1 (SPEI$_{anomaly}$ ≤ −1), and (3) the CWD standard deviation ≤ −1 (CWD$_{anomaly}$ ≤ −1). Any given pixel was classified as drought only when it met two of the above three criteria. For each grid cell, the $X_{anomaly}$ was smoothed using a 3-month running average to avoid a single wet month interrupting a long and consecutive dry period. As a precaution, we excluded those pixels with a short drought period (duration <3 months) to avoid potential data disturbances.

$$X_{anomaly} = \frac{X_t - \overline{X_t}}{\sigma\left(X_t\right)}, \quad (1)$$

where X_t is the drought index (i.e., PDSI, SPEI, and CWD) of month t, $X_{anomaly}$ is the standardized anomaly of X_t, $\overline{X_t}$, and $\sigma\left(X_t\right)$ are the mean and standard deviation (SD) of X_t values from 1988 to 2015.

Then, we calculated the regional percentage of drought pixels (hereafter denoted Drought$_{fraction}$) for the Amazon region, Africa, and Asia in each year to generate the yearly Drought$_{fraction}$ time series in each of the three regions. Subsequently, we used an empirical threshold of Drought$_{fraction}$ exceeding 20% (red circles, Figure S1) to define the drought year for the whole Amazon, Africa, and Asia regions, respectively. The results indicated that Drought$_{fraction}$ peaks exceeding 20% (red circles, Figure S1) generally coincide well with historical drought events, as previously reported (Table S2) for the regions under study. In contrast, the years with minimum values of Drought fraction (i.e., with minimum drought pixels) between two consecutive drought years were categorized as non-drought years (blue circles, Figure S1).

2.4 | Evaluation of the sensitivity of Ku-VOD to top-canopy (TOC) LAI

In this study, we used an LAI product derived from LIDAR signals from GLAS available from 2003 to 2007 (Tang & Dubayah, 2017) as the reference, which is a robust dataset of LAI in tropical evergreen forests (Tang et al., 2016). We selected the footprint data with canopy height ≥15 m for tropical evergreen forests and followed Tang's method (Tang & Dubayah, 2017) to aggregate LIDAR LAI estimates into 0.5-degree pixels with each grid having more than 10 footprint data. Only LIDAR LAI estimates for vertical heights >10 m were included for each pixel to represent TOC LAI (LAI$_{top\ canopy}$). Finally, we conducted a correlation analysis between Ku-VOD and LAI$_{top\ canopy}$ (Figure S4) and compared their mean seasonality in the regions under study (Figure S5).

2.5 | Calculating drought-induced loss and non-drought gain in canopy mass

First, we removed the effects of seasonal variations on the inter-annual variations of Ku-VOD by subtracting the corresponding multiple-year monthly average value of each pixel. We detected the

seasonal cycle of Ku-VOD for each pixel using power spectral analysis (Bradley et al., 2011; Chen et al., 2020). The results showed that the seasonal cycle of Ku-VOD in most pixels followed a 6-month or an annual cycle (Figure S6), suggesting that both maximum and minimum values of monthly Ku-VOD occurred within a 1-year cycle. To avoid a potential delay in the impact of drought on Ku-VOD, the drought period and half of the seasonal cycle post-drought period are collectively referred to as the drought evaluation period (Figure S7A) in analyzing the impact of drought on Ku-VOD. Correspondingly, the time periods from half of the seasonal cycle before the onset of non-drought to the postponed half of the seasonal cycle after the end of the non-drought period are collectively referred to as the non-drought evaluation period (Figure S7B). Finally, we calculated the drought-induced loss in the canopy (ΔKu-VOD$_{drought}$) using the value of deseasonalized Ku-VOD in the drought evaluation periods (red point in Figure S7A) minus the corresponding value in non-drought evaluation periods (blue point in Figure S7B). In turn, the non-drought gain (ΔKu-VOD$_{non\text{-}drought}$) was calculated by subtracting the value of deseasonalized Ku-VOD in the drought evaluation periods (red point in Figure S7A) from the corresponding value in the non-drought evaluation periods (blue point in Figure S7B). The process was conducted at the pixel level for each drought event, and all datasets were aggregated at 0.5° spatial and monthly temporal resolutions based on bilinear interpolation and standard calculation methods.

$$\Delta \text{Ku - VOD}_{\text{drought}} = \frac{\overline{\text{Ku - VOD}_{\text{drought}} - \text{Ku - VOD}_{\text{pre}}}}{\overline{\text{Ku - VOD}^{\text{ori}}_{\text{pre}}}} \times 100\%, \quad (2)$$

$$\Delta \text{Ku - VOD}_{\text{non - drought}} = \frac{\overline{\text{Ku - VOD}_{\text{post}} - \text{Ku - VOD}_{\text{drought}}}}{\overline{\text{Ku - VOD}^{\text{ori}}_{\text{post}}}} \times 100\%, \quad (3)$$

where $\text{Ku - VOD}_{\text{drought}}$ is the value of the deseasonalized Ku-VOD in a drought evaluation period (red point in Figure S7A); $\text{Ku - VOD}_{\text{pre}}$ and $\text{Ku - VOD}_{\text{post}}$ are the values of the deseasonalized Ku-VOD in the non-drought evaluation period before and after the given drought years (blue point in Figure S7B), respectively; $\text{Ku - VOD}^{\text{ori}}_{\text{pre}}$ and $\text{Ku - VOD}^{\text{ori}}_{\text{post}}$ are the original values of Ku-VOD corresponding to $\text{Ku - VOD}_{\text{pre}}$ and $\text{Ku}_{\text{VOD}_{\text{post}}}$, respectively; $\overline{\text{Ku - VOD}_{\text{drought}} - \text{Ku - VOD}_{\text{pre}}}$ and $\overline{\text{Ku - VOD}_{\text{post}} - \text{Ku - VOD}_{\text{drought}}}$ are the mean values of absolute changes during each drought and post-/non-drought event, respectively; and $\overline{\text{Ku - VOD}^{\text{ori}}_{\text{pre}}}$ and $\overline{\text{Ku - VOD}^{\text{ori}}_{\text{post}}}$ are the mean values of $\text{Ku - VOD}^{\text{ori}}_{\text{pre}}$ and $\text{Ku - VOD}^{\text{ori}}_{\text{post}}$, respectively.

We used Equation (4) to evaluate whether Ku-VOD recovered to the same value as that in the non-drought year before each drought event. The corresponding difference (e.g., ΔPDSI$_{Net}$, Figure S8) between the pre- and post- non-drought years is approximately equal to zero, and the value remains stable with increasing Hc. Therefore, ΔNet is minimally affected by canopy water-content differences but is largely related to canopy mass loss.

$$\Delta \text{Net} = \frac{\overline{\text{Ku - VOD}_{\text{post}}} - \overline{\text{Ku - VOD}_{\text{pre}}}}{\overline{\text{Ku - VOD}^{\text{ori}}_{\text{pre}}}} \times 100\% \quad (4)$$

where $\overline{\text{Ku - VOD}_{\text{pre}}}$ and $\overline{\text{Ku - VOD}_{\text{post}}}$ are the mean values of each non-drought evaluation period before and after the given drought year, respectively; negative and positive values represent whether the canopy mass has recovered or not, respectively.

2.6 | Comparing differences in physiological performance using in-situ observations

To assess the dependence of sap flow density on tree height, we collected in-situ sap flow observations from four SAPFLUXNET sites (Poyatos et al., 2021) located in tropical regions with measured Hc (Table S3). We calculated daytime (from 6:00 AM to 6:00 PM local time) mean sap flow of each sample (tree). In addition, we also collected all the in-situ P_{50} datasets of tropical broadleaved evergreen forests from Liu et al. (2019) to study the dependence of hydraulic trait differences on Hc. We then conducted a meta-analysis of mean daytime sap flow and maximum -P_{50} against average Hc of tropical forests using polynomial regression (Ostertagová, 2012) fitted to the data (Figure 2a,b).

2.7 | Relating Ku-VOD dynamics to climatic variables

We further analyzed the Ku-VOD inter-annual variability (ΔKu-VOD) of tropical broadleaved evergreen forests against climatic changes during all drought and non-drought periods defined as described above. Soil water deficit was evaluated by two variables: GRACE terrestrial water storage (TWS; Humphrey & Gudmundsson, 2019) and CRUNCEP precipitation (PRE; Viovy, 2018), while atmospheric dryness was evaluated by ERA-Interim VPD (Yuan et al., 2019; Table S4). We investigated tall tropical forests ($Hc_{Simard} \geq 35.0$ m or $Hc_{GEDI} \geq 27.9$ m) and short tropical forests ($Hc_{Simard} < 35.0$ m or $Hc_{GEDI} < 27.9$ m) to compare the different climatic drivers of the response of ΔKu-VOD to drought in each case (Figure 3, Figure S9, Table S5).

3 | RESULTS

The relative changes in PDSI between each drought and non-drought year-pair showed no significant differences across tropical forests for different Hc classes (Figure S8), implying similar extents of exposure of taller and shorter forests to drought. However, the impact of drought was greater in taller tropical forests having more negative values of ΔKu-VOD$_{drought}$ during drought periods (Figure 1a and red boxplots in Figure 1c). Nonetheless, taller tropical forests recovered faster from drought, with more positive values of ΔKu-VOD$_{non\text{-}drought}$ (Figure 1b and blue boxplots in Figure 1c), than shorter forests.

The Ku-VOD values showed a positive correlation with LIDAR TOC LAI ($LAI_{top\ canopy}$; Figure S4); furthermore, regional averages of Ku-VOD in Amazon, Congo, and tropical Asia were consistent with those of LIDAR $LAI_{top\ canopy}$ in seasonality (Figure S5).

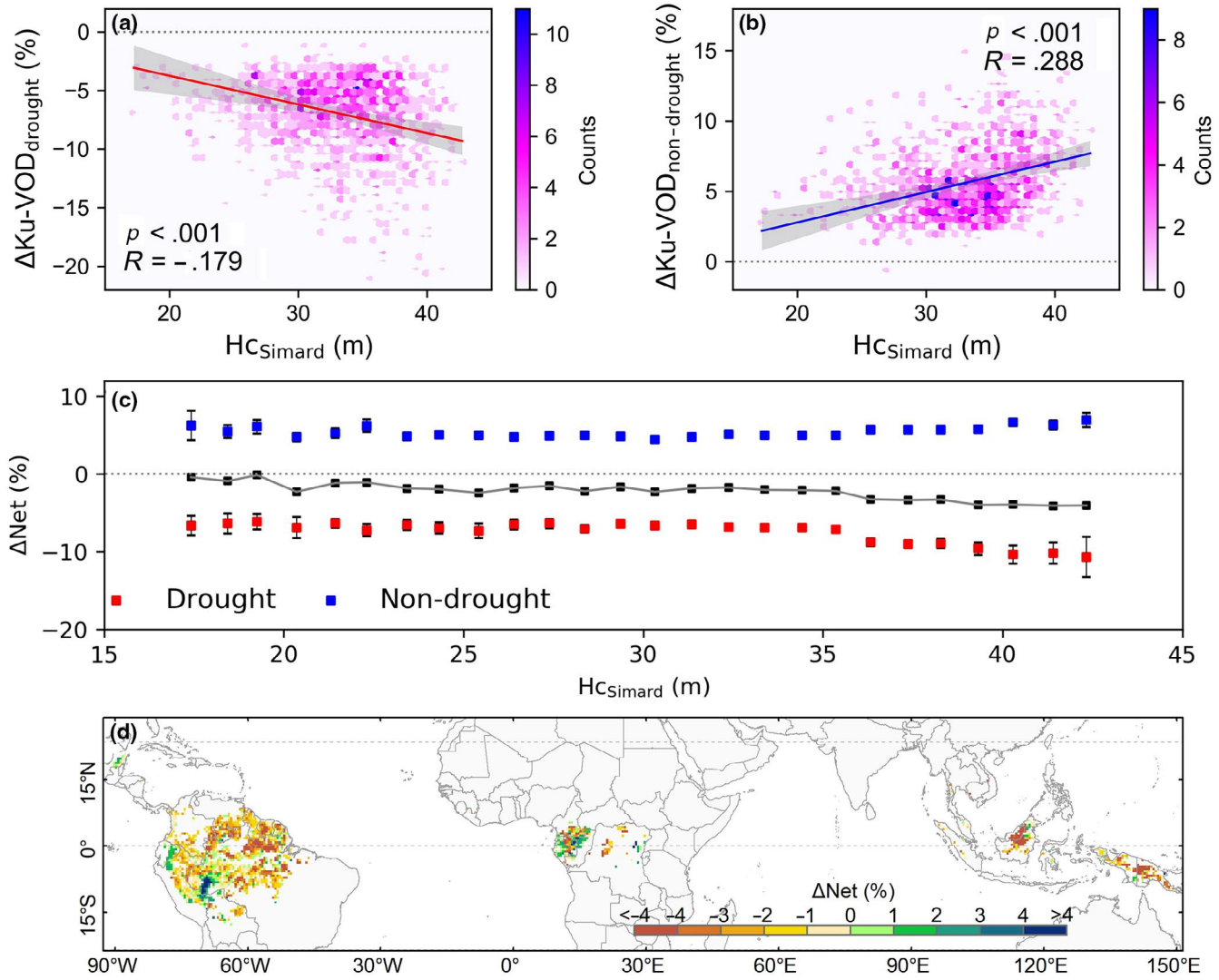

FIGURE 1 Responses of Ku-VOD change of tropical forests to drought against GLAS (geoscience laser altimeter system) LIDAR canopy height (Hc_{Simard}). (a) Bidimensional histogram of pixel-level relative drought-induced loss per drought year (ΔKu-$VOD_{drought}$, unit: %, Equation 2) against GLAS LIDAR Hc. (b) Same for pixel-level relative non-drought gain per non-drought year (ΔKu-$VOD_{non\text{-}drought}$, unit: %, Equation 3). Each dot represents the relative Ku-VOD change of one pixel in each drought (or non-drought) event. The red and blue curves are the corresponding linear fits of the scatters, and the gray shading represents the 95% confidence interval. (c) Statistics (mean ± SEM) of average relative ΔKu-$VOD_{drought}$ (red) and ΔKu-$VOD_{non\text{-}drought}$ (blue) in tropical forests against Hc_{Simard} using one-meter bins. The black curve is the relative ΔNet (%) for each Hc_{Simard} bin. (d) Spatial pattern of the average relative ΔNet in the tropical Amazon, Africa, and Asia. For each pixel, ΔNet is the difference in Ku-VOD between the post-/pre-drought non-drought years (Equation 4) [Colour figure can be viewed at wileyonlinelibrary.com]

When testing the presence of potential breakpoints (Hu et al., 2020) for the relationship between Hc_{Simard}, Hc_{GEDI}, and ΔKu-VOD across space, we found that forests with Hc greater than a threshold value (Hc_{Simard} > 35.0 m; Hc_{GEDI} > 27.9 m) experienced significantly larger ΔKu-$VOD_{drought}$ losses during drought years (Figure S10A,C), and significantly larger ΔKu-$VOD_{non\text{-}drought}$ gains during non-drought years (Figure S10B,D) than forests with Hc below the same threshold values, which incidentally, varied little among the three tropical continental regions (Figure S11). Despite an underestimation of Hc by Hc_{GEDI} (Potapov et al., 2021; Figure S12, mean underestimation = −7.26 ± 0.08 m), results from Hc_{GEDI} were similar to those from Hc_{Simard}.

We further evaluated whether the canopy of tropical forests with different Hc recovered to pre-drought levels, as quantified by the Ku-VOD signal, during the following non-drought period. For each pixel, we calculated the net differences in Ku-VOD (ΔNet; Methods) and PDSI ($\Delta PDSI_{Net}$) between the pre-drought and non-drought years. The value for $\Delta PDSI_{Net}$ proved stable with increasing Hc, approximately equal to zero (Figure S8), implying that ΔNet must be largely related to canopy mass differences and not to differences in the extent of exposure to drought; furthermore, ΔNet showed increasingly negative values with increasing Hc_{Simard} across the pan-tropics (black curve, Figure 1c), suggesting an increase in vulnerability to drought with Hc. Across the pan-tropics, ΔNet becomes more

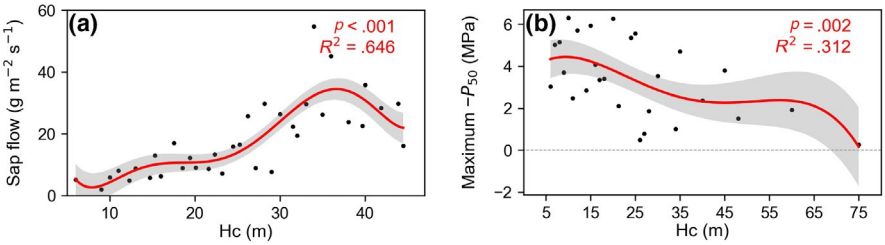

FIGURE 2 Sap flow and stem water potential at 50% loss of conductivity (P_{50}) as a function of tree height in pantropical forests. (a) Mean daytime sap flow of 89 in situ observations for different tree heights (bin is 1.0 m); (b) Maximum -P_{50} of 182 in situ observations for different tree heights (bin is 1.0 m). The scatter diagrams of all 89 in situ sap-flow observations and 182 in situ -P_{50} observations are shown in Figure S16. We excluded the data of Hc shorter than 5.0 m to eliminate possible effects from young forests. The red curves show the corresponding fitted fifth-order polynomials; shading areas represent a 95% confidence interval [Colour figure can be viewed at wileyonlinelibrary.com]

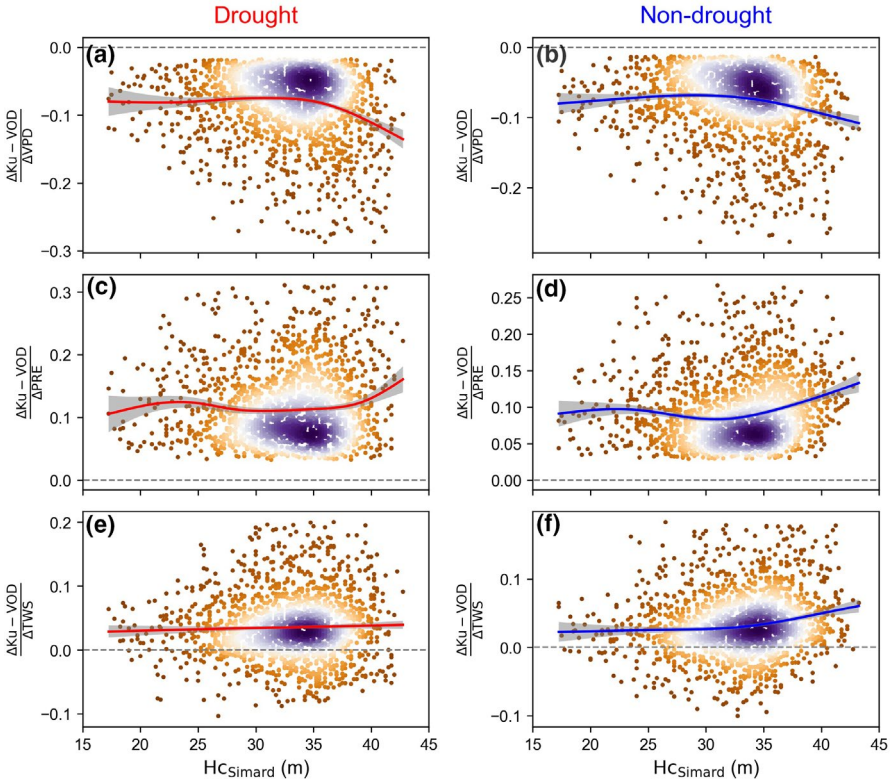

FIGURE 3 Sensitivity of Ku-VOD to VPD, PRE and TWS as functions of forest Hc (Hc_{Simard}). The left column (a, c, and e) denotes drought periods (unit less), and the right column (b, d, and f) denotes non-drought periods (unit less). Red and blue curves were fitted by generalized additive models (GAMs; Yee & Mitchell, 1991). Shaded areas represent a 95% confidence interval. The corresponding statistics of tall and short forests are shown in Table S5 [Colour figure can be viewed at wileyonlinelibrary.com]

negative when Hc_{Simard} ≥ 35.0 m in both the Amazon region and Asia, whereas there was no clear trend observed for Africa (Figure S13). The corresponding forest areas with negative ΔNet were 80%, 54%, and 88% of drought-affected areas, which experienced both drought-induced loss and subsequent non-drought gain, in the Amazon region, Africa, and Asia (Figure 1D), respectively. Again, results from Hc_{GEDI} supported the hypothesis that taller tropical forests showed more relative negative values of $\Delta Ku\text{-}VOD_{drought}$, more positive values of $\Delta Ku\text{-}VOD_{non\text{-}drought}$, and more negative values of ΔNet (Figures S14 and S15), than shorter tropical forests.

In situ observations of eco-physiological factors over tropical continental regions can enhance our understanding of drought impacts on tropical forests. A meta-analysis of in situ daytime sap flow from a total of 89 tropical evergreen broadleaved trees from four SAPFLUXNET sites (Figure S16A, Table S3) showed that sap-flow density (i.e., transpiration capacity) of tropical trees was generally lower when Hc was greater than 35.0 m (Figure 2a). Another meta-analysis of in situ hydraulic traits from 182 tropical evergreen broadleaved trees in Liu et al. (2019; Figure S16B) showed a smaller maximum -P_{50} (i.e., the water potential at which 50% loss of xylem conductivity occurs) for taller trees (Figure 2b), suggesting a greater vulnerability of xylem tissue to embolism under drought conditions in taller trees than in shorter ones, as reported by Rowland et al. (2015) for the Caxiuana drought experiment. It is noteworthy that both sap flow and maximum -P_{50} decreased in tropical forests with increasing Hc over ~35.0 m (Figure 2a,b), consistent with the satellite-based Ku-VOD analysis, which showed that ΔNet became more negative when Hc_{Simard} ≥ ~35.0 m (Figure 1c).

We further analyzed ΔKu-VOD against changes (Δ) in water availability from relative changes in precipitation (ΔPRE), GRACE

terrestrial water storage estimates (ΔTWS), and VPD (ΔVPD; Table S4; Figure 3). The results indicated that the response of ΔKu-VOD to ΔVPD is curvilinear as a function of Hc during both drought and non-drought periods. Taller forests (Hc_{Simard} ≥ 35.0 m) had slightly more negative sensitivity to ΔVPD (during drought years: −0.091 ± 0.002 and during non-drought years: −0.084 ± 0.002) than shorter forests (during drought years: −0.077 ± 0.001 and during non-drought years: −0.070 ± 0.001; Figure 3a,b, Table S5). In contrast, the sensitivity of Ku-VOD to PRE was more positive in taller forests (drought years: 0.118 ± 0.002; non-drought years: 0.102 ± 0.002) than in shorter forests (drought years: 0.114 ± 0.002; non-drought years: 0.088 ± 0.001; Figure 3c,d, Table S5). The Ku-VOD of taller forests was significantly more positively sensitive to ΔTWS (0.042 ± 0.002) than that of shorter forests (0.028 ± 0.001) during non-drought years, while showing similar sensitivity to shorter forests during drought years (taller forests: 0.036 ± 0.002; shorter forests: 0.035 ± 0.001; Figure 3e,f, Table S5). Results based on Hc_{GEDI} showed the same trends (Figure S9, Table S5).

4 | DISCUSSION

At the ecosystem scale, our analysis showed both greater relative Ku-VOD losses during droughts and subsequently stronger relative non-drought gains in taller tropical forests than in shorter ones. The net relative differences in Ku-VOD were more negative in taller tropical forests. Taller trees exhibited lower mean evapotranspiration per unit basal area than shorter trees during drought and were more sensitive to water stress due to their lower xylem-safety margin (i.e., lower maximum $-P_{50}$; Figure 2b). Taller trees reportedly showed higher drought-related mortality (Anderegg et al., 2016; Brando, 2018; Phillips et al., 2010).

The hydraulic failure and carbon starvation hypotheses are two main non-mutually exclusive theories to explain drought-induced dynamics of tropical forests because of significant carbon–hydraulic interactions (Hartmann, 2011; Kono et al., 2019; McDowell et al., 2008; Sala et al., 2010; Zeppel et al., 2013). As shown in Figure 4, under moderate water stress, leaf stomatal closure and leaf shedding are initial responses of trees to mitigate the risk of xylem embolism by reducing the transpiring surface area (Aguadé et al., 2015; Brodribb & Holbrook, 2003; Yazaki et al., 2015), especially in trees with smaller values of $-P_{50}$. Generally, taller trees show smaller Huber values, that is, sapwood area divided by total leaf area (Kono et al., 2019), thus showing proportionally more leaves supported by the same area of xylem than shorter trees (Liu et al., 2019; McDowell et al., 2002). Additionally, taller trees preferentially extract water from deep soil layers (below 100 cm), while shorter trees show broad variations in the depth of water uptake during drought periods (Stahl et al., 2013). Thus, taller forests likely experience higher hydraulic stress, despite having access to deeper soil water due to their longer roots. The reduction in total water consumption by taller trees is more severe under drought conditions than that of shorter trees (Liu et al., 2021). Therefore, although taller trees have relatively wider vessels and the potential for higher water conductivity (Liu et al., 2019; Olson et al., 2018), taller trees are more vulnerable to xylem embolism and are thus at a higher risk of hydraulic failure than shorter trees (Anderegg et al., 2016; Liu et al., 2019).

The above-mentioned intrinsic eco-physiological variations associated with tree height in tropical forests might exert a strong effect on forest canopy growth and photosynthetic dynamics during

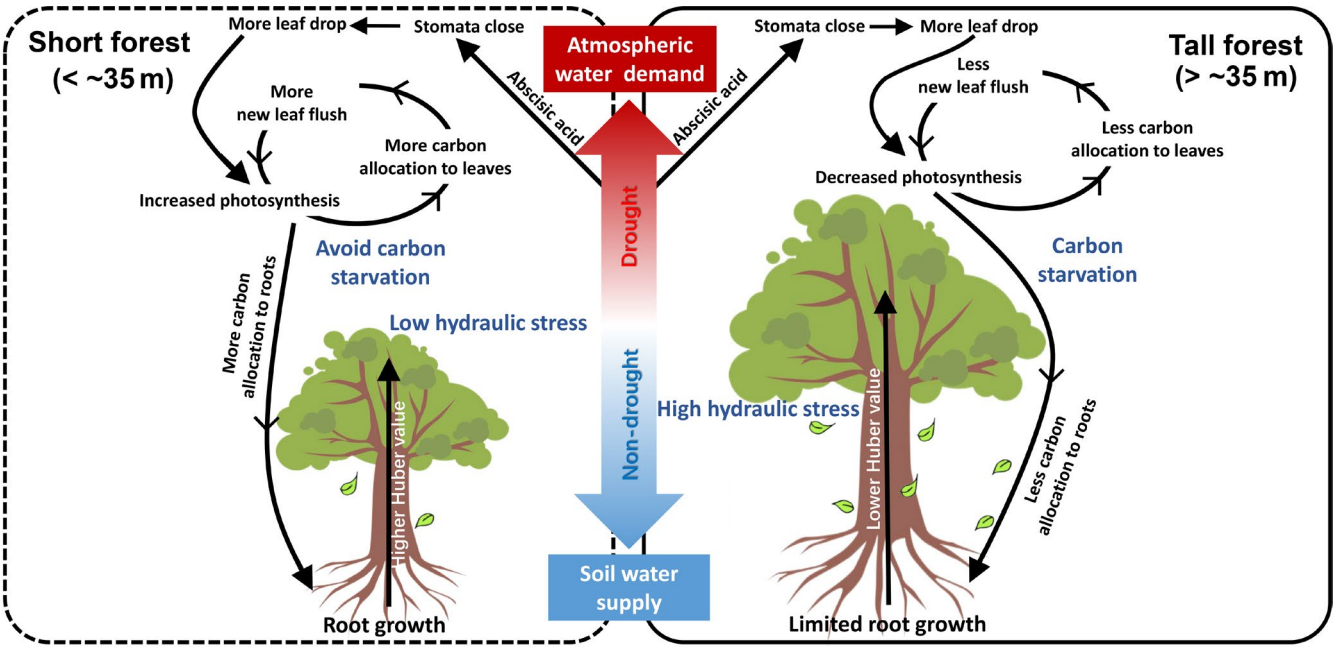

FIGURE 4 An illustration of potential eco-physiological processes in short (Hc < 35.0 m) and tall tropical forests (Hc > 35.0 m) explaining the different responses of canopy dynamics to drought. Huber value = sapwood area/total leaf area [Colour figure can be viewed at wileyonlinelibrary.com]

the drought periods (Figure 4). Trees first increase carbon allocation to leaves and then to roots under water stress (Chen et al., 2020). For example, when Amazonian evergreen forests enter the early dry season, the allocation of carbohydrates to new leaves was found to increase immediately (Poorter et al., 2012). However, the allocation to roots decreased first during the early dry season and increased in the latter part of the dry season (Doughty et al., 2015; Poorter et al., 2012). As taller trees experience greater hydraulic stress, they readily drop more leaves, produce fewer new leaves, and decrease canopy photosynthesis, which in turn causes insufficient carbon allocation to roots during the late stages of the dry season, thereby limiting tree capacity to absorb water from deeper soil layers. This feedback response can lead to hydraulic failure, carbon starvation, or both (Kono et al., 2019). In contrast, canopies of shorter trees experience less hydraulic stress than taller forests, whereby, they are able to replace old leaves with new leaves due to sufficient sunlight, which in turn boosts canopy photosynthesis during drought periods (Chen et al., 2021; Green et al., 2020), thus providing additional carbon which is allocated for root growth into deeper soil for water uptake during the latter part of the dry season (Chen et al., 2020).

Previous studies found that solar-induced fluorescence of taller forests was less sensitive to precipitation than that of shorter ones (Giardina et al., 2018), implying that photosynthesis of taller forests was presumably less sensitive to variations in precipitation than shorter forests. However, photosynthesis of taller forests was more sensitive to atmospheric dryness (Brando, 2018; Giardina et al., 2018; Guan et al., 2015). Our findings suggested that taller forests probably had a higher sensitivity to atmospheric dryness and a higher recovery potential to enhance water absorption than shorter forests (Figure 3). The differences between previous reports and our own could be reconciled by noting that we only focused on drought, when taller forests might allocate insufficient carbon for root growth and leaf flushing, thereby leading to a higher risk of hydraulic failure and carbon starvation than in shorter forests that had a more positive value of ΔNet than taller forests. The relatively shorter forests were distributed mostly over the Amazon (average Hc_{Simard} = 32 m, 67% of pixels with Hc_{Simard} < 35 m) and tropical Africa (average Hc_{Simard} = 33 m, 60% of pixels with Hc_{Simard} < 35 m), where the average canopy height of forests was shorter than in tropical Asia (average Hc_{Simard} = 36 m, 61% of pixels with Hc_{Simard} > 35 m). Additionally, non-equatorial tropical forests in the Amazon region (latitude ≥ 5°S or latitude ≥ 5°N; green and blue regions, Figure 1d) showed more positive values of ΔNet in response to drought than equatorial forests (5°S < latitude < 5°N). We hypothesize that forests with marked seasonal cycles might mitigate drought-induced effects better than low-latitudinal forests near the equator, with slight seasonality of canopy phenology and photosynthesis (Figure S17). Yang, Wu, et al. (2021) observed that non-equatorial forests showed stronger seasonality of leaf fall and photosynthesis, which were mainly controlled by a marked seasonality of sunlight and rainfall (Li et al., 2021; Wagner et al., 2016, 2017). Thus, we inferred that near-equatorial forests might be more influenced by local disturbances (e.g., wind and drought) and differences among plant species (De Queiroz et al., 2019; Guo et al., 2019).

Additionally, our results highlight the need to incorporate water transport as a function of canopy height in land surface models (LSMs) in addition to stomatal conductance and soil water deficit impacts on plant growth (Baker et al., 2008; Markewitz et al., 2010). Analysis of the results of eight dynamic global vegetation models (DGVMs) from the Trendy-v7 exercise (Le Quéré et al., 2018) showed that drought-induced canopy losses and post-drought gains in the modeled canopy leaf area index (LAI; Figures S18 and S19) were not sensitive to satellite Lidar-derived Hc across pantropical forests or even opposite to the response recorded in this study, based on Ku-VOD observations (Figure 1c). As Ku-VOD was sensitive to the LAI top canopy, we compared the modeled LAI with satellite Ku-VOD. The results showed that LAI simulated by those models (Figure S20A,B,D–H), which used dynamic or prescribed Hc (Table S6), were positively and linearly correlated with Ku-VOD. However, the models that did not consider Hc (Figure S20C) performed poorly in simulating LAI in tropical forests. Satellite observations from microwave Ku-VOD showed greater canopy mass losses ($\Delta Ku\text{-}VOD_{drought}$) during drought and greater post-non-drought canopy mass gains ($\Delta Ku\text{-}VOD_{non\text{-}drought}$; Figure S21). Previous studies also observed bidirectional drought-related canopy dynamics in tropical forests in response to drought using multiple satellite-based estimates (Liu et al., 2021). Liu et al. (2021) found that tropical forests with higher background LAI, usually taller trees, decreased canopy LAI during drought periods, and increased canopy LAI faster during the recovery period. In contrast, tropical forests with lower background LAI increased canopy LAI during the drought period and decreased canopy LAI during the recovery period. Therefore, we analyzed the modeled $\Delta LAI_{drought}$ and $\Delta LAI_{non\text{-}drought}$ against background LAI (Figure S22) to test whether LSMs can capture the bidirectional drought-related canopy dynamics of tropical forests. The results showed that only the SDGVM model, which accounts for the effects of Hc on transpiration and LAI (Table S6), captures similar patterns (Figure S22O,P) of ΔKu-VOD against background Ku-VOD (Figure S21). However, CLASS-CTEM, JSBACH, and ORCHIDEE-TRUNK models show that both $\Delta LAI_{drought}$ and $\Delta LAI_{non\text{-}drought}$ decreased as background LAI increased (Figure S22C–F,M–N). CABLE-POP, JULES-ES, LPJ-GUESS, and ORCHIDEE-CNP models showed no significant trend in $\Delta LAI_{drought}$ and $\Delta LAI_{non\text{-}drought}$ as background LAI increased (Figure S22A,B,G–L). Hence, by neglecting to account for the effects of forest canopy height, LSMs tend to underestimate the impact of drought on tall forests and to overestimate it for short forests.

It is worth noting that the drought-induced loss in Ku-VOD ($\Delta Ku\text{-}VOD_{drought}$) can be caused by a decrease in leaf water content, defoliation, or canopy damage (Anderson et al., 2010; Borchert, 1998; Saatchi et al., 2013), while the net loss in Ku-VOD (black dots) during recent drought more likely reflects the part of canopy-mass loss caused by a structural change such as branch snapping and mortality (Brando et al., 2019; Leitold et al., 2018). Similarly, it should be noted that, compared with lower-frequency VOD data, such as L-band

VOD data, which normally shows a higher correlation with aboveground biomass (Brandt et al., 2018; Fan et al., 2019; Wigneron et al., 2020), the Ku-band VOD obtained from higher-frequency passive microwave satellite sensors contains less information of deeper vegetation layers (Chaparro et al., 2018); therefore, it is more related to canopy mass and water content than to stem biomass changes (Ferrazzoli & Guerriero, 1996; Momen et al., 2017; Rodríguez-Fernández et al., 2018; Wigneron et al., 1995, 2004; Zhang et al., 2019). The evaluation of Ku-VOD data based on Lidar LAI (Figures S4 and S5) also proved that Ku-VOD was positively correlated with $LAI_{top\ canopy}$ in tropical forests. Finally, we recommend that future studies combine Ku- and L-band VOD data to separate canopy and stem biomass changes to better understand the responses of tropical forests to drought.

ACKNOWLEDGMENTS

We thank Dr. Bruno Hérault from CIRAD for his constructive suggestions on this paper. This study was supported by the Guangdong Major Project of Basic and Applied Basic Research (grant number 2020B0301030004), the National Natural Science Foundation of China [grant numbers 31971458, 41971275], ECOPROPHET PROJECT [Belspo Stereo3 program (contract SR/00/334)], Special high-level plan project of Guangdong Province [grant number 2016TQ03Z354].

CONFLICT OF INTEREST

The authors declare no competing financial interests.

AUTHOR CONTRIBUTIONS

Xiuzhi Chen, Philippe Ciais, Wenping Yuan, and Yongxian Su designed the study. Xiuzhi Chen, Liyang Liu, Xueqin Yang, and Fanxi Gong collected and analyzed the data and elaborated the figures. All authors contributed to writing and editing the text and discussing the scientific questions.

DATA AVAILABILITY STATEMENT

The Ku-band vegetation optical depth (Ku-VOD) data are available at https://doi.org/10.5281/zenodo.2575599; MODIS land cover map are available at https://modis.gsfc.nasa.gov/data/dataprod/mod12.php; Hansen forest cover map are available at https://earthenginepartners.appspot.com/science-2013-global-forest; CRUNCEP precipitation (PRE) data are available at http://rda.ucar.edu/datasets/ds314.3/; Palmer drought severity index (PDSI) data from Terraclimate are available at https://www.climatologylab.org/terraclimate.html; Standardized precipitation evapotranspiration index (SPEI) from SPEIbase v.2.6 are available at https://spei.csic.es/database.html; The GLAS LIDAR canopy height map (HcSimard) is available at https://webmap.ornl.gov/wcsdown/dataset.jsp?ds_id=10023; The GEDI LIDAR canopy height map (HcGEDI) is available at https://glad.umd.edu/dataset/gedi; The GLEAM Evapotranspiration data used to calculate climatological water deficit (CWD) are available at https://www.gleam.eu/; ERA-Interim data used to calculate vapor pressure deficit (VPD) are available at https://apps.ecmwf.int/datasets/; The reconstructed GRACE terrestrial water storage (TWS) data are available at https://doi.org/10.6084/m9.figshare.7670849.v3; The SAPFLUXNET data are available at https://doi.org/10.5281/zenodo.2530798; P50 data used in this study are available at https://doi.org/10.5281/zenodo.5710219; Datasets to generate figures are available at https://doi.org/10.5281/zenodo.5741273.

ORCID

Liyang Liu https://orcid.org/0000-0002-3663-7981
Xiuzhi Chen https://orcid.org/0000-0003-2375-9995
Philippe Ciais https://orcid.org/0000-0001-8560-4943
Wenping Yuan https://orcid.org/0000-0002-1469-4395
Fabienne Maignan https://orcid.org/0000-0001-5024-5928
Jin Wu https://orcid.org/0000-0001-8991-3970
Shilong Piao https://orcid.org/0000-0001-8057-2292
Ying-Ping Wang https://orcid.org/0000-0002-4614-6203
Jean-Pierre Wigneron https://orcid.org/0000-0001-5345-3618
Lei Fan https://orcid.org/0000-0002-1834-5088
Pierre Gentine https://orcid.org/0000-0002-0845-8345
Xueqin Yang https://orcid.org/0000-0001-8445-2802
Fanxi Gong https://orcid.org/0000-0001-7970-4606
Hui Liu https://orcid.org/0000-0003-4027-499X
Chen Wang https://orcid.org/0000-0003-2706-3549
Xuli Tang https://orcid.org/0000-0002-4498-9485
Hui Yang https://orcid.org/0000-0001-6454-8954
Qing Ye https://orcid.org/0000-0001-5445-0996
Bin He https://orcid.org/0000-0002-9088-262X
Jiali Shang https://orcid.org/0000-0001-9114-1500
Yongxian Su https://orcid.org/0000-0003-2114-628X

REFERENCES

Abatzoglou, J. T., Dobrowski, S. Z., Parks, S. A., & Hegewisch, K. C. (2018). TerraClimate, a high-resolution global dataset of monthly climate and climatic water balance from 1958–2015. *Scientific Data*, *5*(1), 1–12. https://doi.org/10.1038/sdata.2017.191

Aguadé, D., Poyatos, R., Gómez, M., Oliva, J., & Martínez-Vilalta, J. (2015). The role of defoliation and root rot pathogen infection in driving the mode of drought-related physiological decline in Scots pine (*Pinus sylvestris* L.). *Tree Physiology*, *35*(3), 229–242. https://doi.org/10.1093/treephys/tpv005

Anderegg, W. R., Klein, T., Bartlett, M., Sack, L., Pellegrini, A. F., Choat, B., & Jansen, S. (2016). Meta-analysis reveals that hydraulic traits explain cross-species patterns of drought-induced tree mortality across the globe. *Proceedings of the National Academy of Sciences of the United States of America*, *113*(18), 5024–5029. https://doi.org/10.1073/pnas.1525678113

Anderson, L. O., Malhi, Y., Aragão, L. E., Ladle, R., Arai, E., Barbier, N., & Phillips, O. (2010). Remote sensing detection of droughts in Amazonian forest canopies. *New Phytologist*, *187*(3), 733–750. https://doi.org/10.1111/j.1469-8137.2010.03355.x

Aragão, L. E. O., Malhi, Y., Roman-Cuesta, R. M., Saatchi, S., Anderson, L. O., & Shimabukuro, Y. E. (2007). Spatial patterns and fire response of recent Amazonian droughts. *Geophysical Research Letters*, *34*(7). https://doi.org/10.1029/2006GL028946

Baccini, A., Walker, W., Carvalho, L., Farina, M., Sulla-Menashe, D., & Houghton, R. A. (2017). Tropical forests are a net carbon source based on aboveground measurements of gain and loss. *Science*, *358*(6360), 230–234. https://doi.org/10.1126/science.aam5962

Baker, I. T., Prihodko, L., Denning, A. S., Goulden, M., Miller, S., & Da Rocha, H. R. (2008). Seasonal drought stress in the Amazon: Reconciling models and observations. *Journal of Geophysical Research Biogeosciences*, *113*(G1). https://doi.org/10.1029/2007JG000644

Barros, F. D. V., Bittencourt, P. R. L., Brum, M., Restrepo-Coupe, N., Pereira, L., Teodoro, G. S., Saleska, S. R., Borma, L. S., Christoffersen, B. O., Penha, D., Alves, L. F., Lima, A. J. N., Carneiro, V. M. C., Gentine, P., Lee, J.-E., Aragão, L. E. O. C., Ivanov, V., Leal, L. S. M., Araujo, A. C., & Oliveira, R. S. (2019). Hydraulic traits explain differential responses of Amazonian forests to the 2015 El Niño-induced drought. *New Phytologist*, *223*(3), 1253–1266. https://doi.org/10.1111/nph.15909

Borchert, R. (1998). Responses of tropical trees to rainfall seasonality and its long-term changes. In A. Markham (Ed.), *Potential impacts of climate change on tropical forest ecosystems* (pp. 241–253). Springer. https://doi.org/10.1007/978-94-017-2730-3_10

Bradley, A. V., Gerard, F. F., Barbier, N., Weedon, G. P., Anderson, L. O., Huntingford, C., Aragão, L. E. O. C., Zelazowski, P., & Arai, E. (2011). Relationships between phenology, radiation and precipitation in the Amazon region. *Global Change Biology*, *17*(6), 2245–2260. https://doi.org/10.1111/j.1365-2486.2011.02405.x

Brando, P. (2018). Tree height matters. *Nature Geoscience*, *11*(6), 390–391. https://doi.org/10.1038/s41561-018-0147-z

Brando, P. M., Paolucci, L., Ummenhofer, C. C., Ordway, E. M., Hartmann, H., Cattau, M. E., Rattis, L., Medjibe, V., Coe, M. T., & Balch, J. (2019). Droughts, wildfires, and forest carbon cycling: A pantropical synthesis. *Annual Review of Earth and Planetary Sciences*, *47*, 555–581. https://doi.org/10.1146/annurev-earth-082517-010235

Brandt, M., Wigneron, J.-P., Chave, J., Tagesson, T., Penuelas, J., Ciais, P., Rasmussen, K., Tian, F., Mbow, C., Al-Yaari, A., Rodriguez-Fernandez, N., Schurgers, G., Zhang, W., Chang, J., Kerr, Y., Verger, A., Tucker, C., Mialon, A., Rasmussen, L. V., … Fensholt, R. (2018). Satellite passive microwaves reveal recent climate-induced carbon losses in African drylands. *Nature Ecology & Evolution*, *2*(5), 827–835. https://doi.org/10.1038/s41559-018-0530-6

Brienen, R. J. W., Gloor, E., Clerici, S., Newton, R., Arppe, L., Boom, A., Bottrell, S., Callaghan, M., Heaton, T., Helama, S., Helle, G., Leng, M. J., Mielikäinen, K., Oinonen, M., & Timonen, M. (2017). Tree height strongly affects estimates of water-use efficiency responses to climate and CO_2 using isotopes. *Nature Communications*, *8*, 288. https://doi.org/10.1038/s41467-017-00225-z

Brodribb, T. J., & Holbrook, N. M. (2003). Stomatal closure during leaf dehydration, correlation with other leaf physiological traits. *Plant Physiology*, *132*(4), 2166–2173. https://doi.org/10.1104/pp.103.023879

Chaparro, D., Piles, M., Vall-Llossera, M., Camps, A., Konings, A. G., & Entekhabi, D. (2018). L-band vegetation optical depth seasonal metrics for crop yield assessment. *Remote Sensing of Environment*, *212*, 249–259. https://doi.org/10.1016/j.rse.2018.04.049

Chen, X., Ciais, P., Maignan, F., Zhang, Y., Bastos, A., Liu, L., Bacour, C., Fan, L., Gentine, P., Goll, D., Green, J., Kim, H., Li, L., Liu, Y. I., Peng, S., Tang, H., Viovy, N., Wigneron, J.-P., Wu, J., … Zhang, H. (2021). Vapor pressure deficit and sunlight explain seasonality of leaf phenology and photosynthesis across Amazonian evergreen broadleaved forest. *Global Biogeochemical Cycles*, *35*(6), e2020GB006893. https://doi.org/10.1029/2020GB006893

Chen, X., Maignan, F., Viovy, N., Bastos, A., Goll, D., Wu, J., Liu, L., Yue, C., Peng, S., Yuan, W., Conceição, A. C., O'Sullivan, M., & Ciais, P. (2020). Novel representation of leaf phenology improves simulation of Amazonian evergreen forest photosynthesis in a land surface model. *Journal of Advances in Modeling Earth Systems*, *12*(1), e2018MS001565. https://doi.org/10.1029/2018MS001565

Cook, B. I., Smerdon, J. E., Seager, R., & Coats, S. (2014). Global warming and 21st century drying. *Climate Dynamics*, *43*(9), 2607–2627. https://doi.org/10.1007/s00382-014-2075-y

da Costa, A. C. L., Galbraith, D., Almeida, S., Portela, B. T. T., da Costa, M., de Athaydes Silva Junior, J., Braga, A. P., de Gonçalves, P. H. L., de Oliveira, A. A. R., Fisher, R., Phillips, O. L., Metcalfe, D. B., Levy, P., & Meir, P. (2010). Effect of 7 yr of experimental drought on vegetation dynamics and biomass storage of an eastern Amazonian rainforest. *New Phytologist*, *187*(3), 579–591. https://doi.org/10.1111/j.1469-8137.2010.03309.x

Dai, A. (2013). Increasing drought under global warming in observations and models. *Nature Climate Change*, *3*(1), 52–58. https://doi.org/10.1038/nclimate1633

de Queiroz, M. G., da Silva, T. G. F., Zolnier, S., de Souza, C. A. A., de Souza, L. S. B., Steidle Neto, A. J., de Araújo, G. G. L., & Ferreira, W. P. M. (2019). Seasonal patterns of deposition litterfall in a seasonal dry tropical forest. *Agricultural and Forest Meteorology*, *279*, 107712. https://doi.org/10.1016/j.agrformet.2019.107712

Doughty, C. E., Metcalfe, D. B., Girardin, C. A. J., Amézquita, F. F., Cabrera, D. G., Huasco, W. H., Silva-Espejo, J. E., Araujo-Murakami, A., da Costa, M. C., Rocha, W., Feldpausch, T. R., Mendoza, A. L. M., da Costa, A. C. L., Meir, P., Phillips, O. L., & Malhi, Y. (2015). Drought impact on forest carbon dynamics and fluxes in Amazonia. *Nature*, *519*(7541), 78–82. https://doi.org/10.1038/nature14213

Fan, L., Wigneron, J.-P., Ciais, P., Chave, J., Brandt, M., Fensholt, R., Saatchi, S. S., Bastos, A., Al-Yaari, A., Hufkens, K., Qin, Y., Xiao, X., Chen, C., Myneni, R. B., Fernandez-Moran, R., Mialon, A., Rodriguez-Fernandez, N. J., Kerr, Y., Tian, F., & Peñuelas, J. (2019). Satellite-observed pantropical carbon dynamics. *Nature Plants*, *5*(9), 944–951. https://doi.org/10.1038/s41477-019-0478-9

Ferrazzoli, P., & Guerriero, L. (1996). Passive microwave remote sensing of forests: A model investigation. *IEEE Transactions on Geoscience and Remote Sensing*, *34*(2), 433–443. https://doi.org/10.1109/36.485121

Frolking, S., Hagen, S., Milliman, T., Palace, M., Shimbo, J. Z., & Fahnestock, M. (2012). Detection of large-scale forest canopy change in pantropical humid forests 2000–2009 with the SeaWinds Ku-band scatterometer. *IEEE Transactions on Geoscience and Remote Sensing*, *50*(7), 2603–2617. https://doi.org/10.1109/TGRS.2011.2182516

Gentine, P., Guérin, M., Uriarte, M., McDowell, N. G., & Pockman, W. T. (2016). An allometry-based model of the survival strategies of hydraulic failure and carbon starvation. *Ecohydrology*, *9*(3), 529–546. https://doi.org/10.1002/eco.1654

Giardina, F., Konings, A. G., Kennedy, D., Alemohammad, S. H., Oliveira, R. S., Uriarte, M., & Gentine, P. (2018). Tall Amazonian forests are less sensitive to precipitation variability. *Nature Geoscience*, *11*(6), 405–409. https://doi.org/10.1038/s41561-018-0133-5

Green, J. K., Berry, J., Ciais, P., Zhang, Y., & Gentine, P. (2020). Amazon rainforest photosynthesis increases in response to atmospheric dryness. *Science Advances*, *6*(47), eabb7232. https://doi.org/10.1126/sciadv.abb7232

Guan, K., Pan, M., Li, H., Wolf, A., Wu, J., Medvigy, D., Caylor, K. K., Sheffield, J., Wood, E. F., Malhi, Y., Liang, M., Kimball, J. S., Saleska, S. R., Berry, J., Joiner, J., & Lyapustin, A. I. (2015). Photosynthetic seasonality of global tropical forests constrained by hydroclimate. *Nature Geoscience*, *8*(4), 284–289. https://doi.org/10.1038/ngeo2382

Guan, K., Wolf, A., Medvigy, D., Caylor, K. K., Pan, M., & Wood, E. F. (2013). Seasonal coupling of canopy structure and function in African tropical forests and its environmental controls. *Ecosphere*, *4*(3), 1–21. https://doi.org/10.1890/ES12-00232.1

Guo, Y., Chen, H. Y., Mallik, A. U., Wang, B., Li, D., Xiang, W., & Li, X. (2019). Predominance of abiotic drivers in the relationship between species diversity and litterfall production in a tropical karst seasonal rainforest. *Forest Ecology and Management*, *449*, 117452. https://doi.org/10.1016/j.foreco.2019.117452

Hansen, M. C., Potapov, P. V., Moore, R., Hancher, M., Turubanova, S. A., Tyukavina, A., Thau, D., Stehman, S. V., Goetz, S. J., Loveland, T. R., Kommareddy, A., Egorov, A., Chini, L., Justice, C. O., &

Townshend, J. R. G. (2013). High-resolution global maps of 21st-century forest cover change. *Science*, *342*(6160), 850–853. https://doi.org/10.1126/science.1244693

Hartmann, H. (2011). Will a 385 million year-struggle for light become a struggle for water and for carbon?—How trees may cope with more frequent climate change-type drought events. *Global Change Biology*, *17*(1), 642–655. https://doi.org/10.1111/j.1365-2486.2010.02248.x

Hérault, B., Beauchêne, J., Muller, F., Wagner, F., Baraloto, C., Blanc, L., & Martin, J. M. (2010). Modeling decay rates of dead wood in a neotropical forest. *Oecologia*, *164*(1), 243–251. https://doi.org/10.1007/s00442-010-1602-8

Hu, A., Wang, J., Sun, H., Niu, B., Si, G., Wang, J., Yeh, C.-F., Zhu, X., Lu, X., Zhou, J., Yang, Y., Ren, M., Hu, Y., Dong, H., & Zhang, G. (2020). Mountain biodiversity and ecosystem functions: Interplay between geology and contemporary environments. *The ISME Journal*, *14*(4), 931–944. https://doi.org/10.1038/s41396-019-0574-x

Humphrey, V., & Gudmundsson, L. (2019). GRACE-REC: A reconstruction of climate-driven water storage changes over the last century. *Earth System Science Data*, *11*(3), 1153–1170. https://doi.org/10.5194/essd-11-1153-2019

Kono, Y., Ishida, A., Saiki, S.-T., Yoshimura, K., Dannoura, M., Yazaki, K., Kimura, F., Yoshimura, J., & Aikawa, S.-I. (2019). Initial hydraulic failure followed by late-stage carbon starvation leads to drought-induced death in the tree *Trema orientalis*. *Communications Biology*, *2*(1), 1–9. https://doi.org/10.1038/s42003-018-0256-7

Le Quéré, C., Andrew, R. M., Friedlingstein, P., Sitch, S., Hauck, J., Pongratz, J., Pickers, P. A., Korsbakken, J. I., Peters, G. P., Canadell, J. G., Arneth, A., Arora, V. K., Barbero, L., Bastos, A., Bopp, L., Chevallier, F., Chini, L. P., Ciais, P., Doney, S. C., … Zheng, B. O. (2018). Global carbon budget 2018. *Earth System Science Data*, *10*(4), 2141–2194. https://doi.org/10.5194/essd-10-2141-2018

Leitold, V., Morton, D. C., Longo, M., dos-Santos, M. N., Keller, M., & Scaranello, M. (2018). El Niño drought increased canopy turnover in Amazon forests. *New Phytologist*, *219*(3), 959–971. https://doi.org/10.1111/nph.15110

Lewis, S. L., Brando, P. M., Phillips, O. L., Van Der Heijden, G. M., & Nepstad, D. (2011). The 2010 amazon drought. *Science*, *331*(6017), 554. https://doi.org/10.1126/science.1200807

Li, Q., Chen, X., Yuan, W., Lu, H., Shen, R., Wu, S., Gong, F., Dai, Y., Liu, L., Sun, Q., Zhang, C., & Su, Y. (2021). Remote sensing of seasonal climatic constraints on leaf phenology across pantropical evergreen forest biome. *Earth's Future*, *9*(9). https://doi.org/10.1029/2021ef002160

Liu, H., Gleason, S. M., Hao, G., Hua, L., He, P., Goldstein, G., & Ye, Q. (2019). Hydraulic traits are coordinated with maximum plant height at the global scale. *Science Advances*, *5*(2), eaav1332. https://doi.org/10.1126/sciadv.aav1332

Liu, J., Bowman, K. W., Schimel, D. S., Parazoo, N. C., Jiang, Z., Lee, M., Bloom, A. A., Wunch, D., Frankenberg, C., Sun, Y., O'Dell, C. W., Gurney, K. R., Menemenlis, D., Gierach, M., Crisp, D., & Eldering, A. (2017). Contrasting carbon cycle responses of the tropical continents to the 2015–2016 El Niño. *Science*, *358*(6360). https://doi.org/10.1126/science.aam5690

Liu, L., Gong, F., Chen, X., Su, Y., Fan, L., Wu, S., Yang, X., Zhang, J., Yuan, W., Ciais, P., & Zhou, C. (2021). Bidirectional drought-related canopy dynamics across pantropical forests: A satellite-based statistical analysis. *Remote Sensing in Ecology and Conservation*. https://doi.org/10.1002/rse2.229

Malhi, Y., Aragao, L. E. O. C., Galbraith, D., Huntingford, C., Fisher, R., Zelazowski, P., Sitch, S., McSweeney, C., & Meir, P. (2009). Exploring the likelihood and mechanism of a climate-change-induced dieback of the Amazon rainforest. *Proceedings of the National Academy of Sciences of the United States of America*, *106*(49), 20610–20615. https://doi.org/10.1073/pnas.0804619106

Malhi, Y., & Grace, J. (2000). Tropical forests and atmospheric carbon dioxide. *Trends in Ecology & Evolution*, *15*(8), 332–337. https://doi.org/10.1016/S0169-5347(00)01906-6

Markewitz, D., Devine, S., Davidson, E. A., Brando, P., & Nepstad, D. C. (2010). Soil moisture depletion under simulated drought in the Amazon: Impacts on deep root uptake. *New Phytologist*, *187*(3), 592–607. https://doi.org/10.1111/j.1469-8137.2010.03391.x

McDowell, N., Barnard, H., Bond, B., Hinckley, T., Hubbard, R., Ishii, H., Köstner, B., Magnani, F., Marshall, J., Meinzer, F., Phillips, N., Ryan, M., & Whitehead, D. (2002). The relationship between tree height and leaf area: Sapwood area ratio. *Oecologia*, *132*(1), 12–20. https://doi.org/10.1007/s00442-002-0904-x

McDowell, N., Pockman, W. T., Allen, C. D., Breshears, D. D., Cobb, N., Kolb, T., Plaut, J., Sperry, J., West, A., Williams, D. G., & Yepez, E. A. (2008). Mechanisms of plant survival and mortality during drought: Why do some plants survive while others succumb to drought? *New Phytologist*, *178*(4), 719–739. https://doi.org/10.1111/j.1469-8137.2008.02436.x

Mencuccini, M., Martínez-Vilalta, J., Vanderklein, D., Hamid, H. A., Korakaki, E., Lee, S., & Michiels, B. (2005). Size-mediated ageing reduces vigour in trees. *Ecology Letters*, *8*(11), 1183–1190. https://doi.org/10.1111/j.1461-0248.2005.00819.x

Mera, Y. E. Z., Vera, J. F. R., & Pérez-Martín, M. Á. (2018). Linking El Niño Southern Oscillation for early drought detection in tropical climates: The Ecuadorian coast. *Science of the Total Environment*, *643*, 193–207. https://doi.org/10.1016/j.scitotenv.2018.06.160

Moesinger, L., Dorigo, W., de Jeu, R., van der Schalie, R., Scanlon, T., Teubner, I., & Forkel, M. (2020). The global long-term microwave vegetation optical depth climate archive (VODCA). *Earth System Science Data*, *12*(1), 177–196. https://doi.org/10.5194/essd-12-177-2020

Momen, M., Wood, J. D., Novick, K. A., Pangle, R., Pockman, W. T., McDowell, N. G., & Konings, A. G. (2017). Interacting effects of leaf water potential and biomass on vegetation optical depth. *Journal of Geophysical Research: Biogeosciences*, *122*(11), 3031–3046. https://doi.org/10.1002/2017JG004145

Nepstad, D. C., Tohver, I. M., Ray, D., Moutinho, P., & Cardinot, G. (2007). Mortality of large trees and lianas following experimental drought in an Amazon forest. *Ecology*, *88*(9), 2259–2269. https://doi.org/10.1890/06-1046.1

Olson, M. E., Soriano, D., Rosell, J. A., Anfodillo, T., Donoghue, M. J., Edwards, E. J., León-Gómez, C., Dawson, T., Camarero Martínez, J. J., Castorena, M., Echeverría, A., Espinosa, C. I., Fajardo, A., Gazol, A., Isnard, S., Lima, R. S., Marcati, C. R., & Méndez-Alonzo, R. (2018). Plant height and hydraulic vulnerability to drought and cold. *Proceedings of the National Academy of Sciences of the United States of America*, *115*(29), 7551–7556. https://doi.org/10.1073/pnas.1721728115

Ostertagová, E. (2012). Modelling using polynomial regression. *Procedia Engineering*, *48*, 500–506. https://doi.org/10.1016/j.proeng.2012.09.545

Palmer, W. C. (1965). *Meteorological drought*. Research Paper No. 45. US Department of Commerce Weather Bureau.

Phillips, O. L., Aragão, L. E. O. C., Lewis, S. L., Fisher, J. B., Lloyd, J., López-González, G., Malhi, Y., Monteagudo, A., Peacock, J., Quesada, C. A., van der Heijden, G., Almeida, S., Amaral, Iêda, Arroyo, L., Aymard, G., Baker, T. R., Bánki, O., Blanc, L., Bonal, D., … Torres-Lezama, A. (2009). Drought sensitivity of the Amazon rainforest. *Science*, *323*(5919), 1344–1347. https://doi.org/10.1126/science.1164033

Phillips, O. L., van der Heijden, G., Lewis, S. L., López-González, G., Aragão, L. E. O. C., Lloyd, J., Malhi, Y., Monteagudo, A., Almeida, S., Dávila, E. A., Amaral, I., Andelman, S., Andrade, A., Arroyo, L., Aymard, G., Baker, T. R., Blanc, L., Bonal, D., de Oliveira, Á. C. A., … Vilanova, E. (2010). Drought–mortality relationships for tropical forests. *New Phytologist*, *187*(3), 631–646. https://doi.org/10.1111/j.1469-8137.2010.03359.x

Poorter, H., Niklas, K. J., Reich, P. B., Oleksyn, J., Poot, P., & Mommer, L. (2012). Biomass allocation to leaves, stems and roots: Meta-analyses of interspecific variation and environmental control. *New Phytologist*, *193*(1), 30–50. https://doi.org/10.1111/j.1469-8137.2011.03952.x

Potapov, P., Li, X., Hernandez-Serna, A., Tyukavina, A., Hansen, M. C., Kommareddy, A., Pickens, A., Turubanova, S., Tang, H., Silva, C. E., Armston, J., Dubayah, R., Blair, J. B., & Hofton, M. (2021). Mapping global forest canopy height through integration of GEDI and Landsat data. *Remote Sensing of Environment*, *253*, 112165. https://doi.org/10.1016/j.rse.2020.112165

Poyatos, R., Granda, V., Flo, V., Adams, M. A., Adorján, B., Aguadé, D., Aidar, M. P. M., Allen, S., Alvarado-Barrientos, M. S., Anderson-Teixeira, K. J., Aparecido, L. M., Arain, M. A., Aranda, I., Asbjornsen, H., Baxter, R., Beamesderfer, E., Berry, Z. C., Berveiller, D., Blakely, B., … Martínez-Vilalta, J. (2021). Global transpiration data from sap flow measurements: the SAPFLUXNET database. *Earth System Science Data*, *13*, 2607–2649. https://doi.org/10.5194/essd-13-2607-2021

Rodríguez-Fernández, N. J., Mialon, A., Mermoz, S., Bouvet, A., Richaume, P., Al Bitar, A., Al-Yaari, A., Brandt, M., Kaminski, T., Le Toan, T., Kerr, Y. H., & Wigneron, J.-P. (2018). An evaluation of SMOS L-band vegetation optical depth (L-VOD) data sets: High sensitivity of L-VOD to above-ground biomass in Africa. *Biogeosciences*, *15*(14), 4627–4645. https://doi.org/10.5194/bg-15-4627-2018

Rowland, L., da Costa, A. C. L., Galbraith, D. R., Oliveira, R. S., Binks, O. J., Oliveira, A. A. R., Pullen, A. M., Doughty, C. E., Metcalfe, D. B., Vasconcelos, S. S., Ferreira, L. V., Malhi, Y., Grace, J., Mencuccini, M., & Meir, P. (2015). Death from drought in tropical forests is triggered by hydraulics not carbon starvation. *Nature*, *528*(7580), 119–122. https://doi.org/10.1038/nature15539

Saatchi, S., Asefi-Najafabady, S., Malhi, Y., Aragão, L. E., Anderson, L. O., Myneni, R. B., & Nemani, R. (2013). Persistent effects of a severe drought on Amazonian forest canopy. *Proceedings of the National Academy of Sciences of the United States of America*, *110*(2), 565–570. https://doi.org/10.1073/pnas.1204651110

Sala, A., Piper, F., & Hoch, G. (2010). Physiological mechanisms of drought-induced tree mortality are far from being resolved. *New Phytologist*, *186*(2), 274–281. https://doi.org/10.1111/j.1469-8137.2009.03167.x

Simard, M., Pinto, N., Fisher, J. B., & Baccini, A. (2011). Mapping forest canopy height globally with spaceborne lidar. *Journal of Geophysical Research: Biogeosciences*, *116*(G4). https://doi.org/10.1029/2011JG001708

Sperry, J. S., Hacke, U. G., Oren, R., & Comstock, J. P. (2002). Water deficits and hydraulic limits to leaf water supply. *Plant, Cell & Environment*, *25*(2), 251–263. https://doi.org/10.1111/j.1744-7429.2012.00902.x

Stahl, C., Burban, B., Wagner, F., Goret, J. Y., Bompy, F., & Bonal, D. (2013). Influence of seasonal variations in soil water availability on gas exchange of tropical canopy trees. *Biotropica*, *45*(2), 155–164. https://doi.org/10.1111/j.1744-7429.2012.00902.x

Sulla-Menashe, D., & Friedl, M. A. (2018). *User guide to collection 6 MODIS land cover (MCD12Q1 and MCD12C1) product* (pp. 1–18). USGS.

Tang, H., & Dubayah, R. (2017). Light-driven growth in Amazon evergreen forests explained by seasonal variations of vertical canopy structure. *Proceedings of the National Academy of Sciences of the United States of America*, *114*(10), 2640–2644. https://doi.org/10.1073/pnas.1616943114

Tang, H., Ganguly, S., Zhang, G., Hofton, M. A., Nelson, R. F., & Dubayah, R. (2016). Characterizing leaf area index (LAI) and vertical foliage profile (VFP) over the United States. *Biogeosciences*, *13*(1), 239–252. https://doi.org/10.5194/bg-13-239-2016

Tyree, M. T., & Sperry, J. S. (1989). Vulnerability of xylem to cavitation and embolism. *Annual Review of Plant Biology*, *40*(1), 19–36. https://doi.org/10.1146/annurev.pp.40.060189.000315

Verbesselt, J., Umlauf, N., Hirota, M., Holmgren, M., Van Nes, E. H., Herold, M., Zeileis, A., & Scheffer, M. (2016). Remotely sensed resilience of tropical forests. *Nature Climate Change*, *6*(11), 1028–1031. https://doi.org/10.1038/nclimate3108

Vicente-Serrano, S. M., Beguería, S., & López-Moreno, J. I. (2010). A multiscalar drought index sensitive to global warming: The standardized precipitation evapotranspiration index. *Journal of Climate*, *23*(7), 1696–1718. https://doi.org/10.1175/2009JCLI2909.1

Vicente-Serrano, S. M., Beguería, S., López-Moreno, J. I., Angulo, M., & El Kenawy, A. (2010). A new global 0.5° gridded dataset (1901–2006) of a multiscalar drought index: Comparison with current drought index datasets based on the palmer drought severity index. *Journal of Hydrometeorology*, *11*(4), 1033–1043. https://doi.org/10.1175/2010JHM1224.1

Viovy, N. (2018). CRUNCEP version 7—Atmospheric forcing data for the community land model. Research Data Archive at the National Center for Atmospheric Research, Computational and Information Systems Laboratory, *10*. https://doi.org/10.5065/PZ8F-F017

Wagner, F. H., Hérault, B., Bonal, D., Stahl, C., Anderson, L. O., Baker, T. R., Becker, G. S., Beeckman, H., Boanerges Souza, D., Botosso, P. C., Bowman, D. M. J. S., Bräuning, A., Brede, B., Brown, F. I., Camarero, J. J., Camargo, P. B., Cardoso, F. C. G., Carvalho, F. A., Castro, W., … Aragão, L. E. O. C. (2016). Climate seasonality limits leaf carbon assimilation and wood productivity in tropical forests. *Biogeosciences*, *13*(8), 2537–2562. https://doi.org/10.5194/bg-13-2537-2016

Wagner, F. H., Hérault, B., Rossi, V., Hilker, T., Maeda, E. E., Sanchez, A., Lyapustin, A. I., Galvão, L. S., Wang, Y., & Aragão, L. E. O. C. (2017). Climate drivers of the Amazon forest greening. *PLoS One*, *12*(7), e0180932. https://doi.org/10.1371/journal.pone.0180932

Wang, X., Piao, S., Ciais, P., Friedlingstein, P., Myneni, R. B., Cox, P., Heimann, M., Miller, J., Peng, S., Wang, T., Yang, H., & Chen, A. (2014). A two-fold increase of carbon cycle sensitivity to tropical temperature variations. *Nature*, *506*(7487), 212–215. https://doi.org/10.1038/nature12915

Wigneron, J. P., Chanzy, A., Calvet, J. C., & Bruguier, N. (1995). A simple algorithm to retrieve soil moisture and vegetation biomass using passive microwave measurements over crop fields. *Remote Sensing of Environment*, *51*(3), 331–341. https://doi.org/10.1016/0034-4257(94)00081-W

Wigneron, J.-P., Fan, L., Ciais, P., Bastos, A., Brandt, M., Chave, J., Saatchi, S., Baccini, A., & Fensholt, R. (2020). Tropical forests did not recover from the strong 2015–2016 El Niño event. *Science Advances*, *6*(6), 2015–2016. https://doi.org/10.1126/sciadv.aay4603

Wigneron, J. P., Pardé, M., Waldteufel, P., Chanzy, A., Kerr, Y., Schmidl, S., & Skou, N. (2004). Characterizing the dependence of vegetation model parameters on crop structure, incidence angle, and polarization at L-band. *IEEE Transactions on Geoscience and Remote Sensing*, *42*(2), 416–425. https://doi.org/10.1109/TGRS.2003.817976

Yang, H., Ciais, P., Chave, J., Huang, Y., Ballantyne, A. P., Yu, K., Berzaghi, F., & Wigneron, J.-P. (2021). Coarse woody debris are buffering mortality-induced carbon losses to the atmosphere in tropical forests. *Environmental Research Letters*, *16*(1), 011006. https://doi.org/10.1088/1748-9326/abd58a

Yang, X., Wu, J., Chen, X., Ciais, P., Maignan, F., Yuan, W., Piao, S., Yang, S., Gong, F., Su, Y., Dai, Y., Liu, L., Zhang, H., Bonal, D., Liu, H., Chen, G., Lu, H., Wu, S., Fan, L., … Wright, S. J. (2021). A comprehensive framework for seasonal controls of leaf abscission and productivity in evergreen broadleaved tropical and subtropical forests. *The Innovation*, *2*(4), 100154. https://doi.org/10.1016/j.xinn.2021.100154

Yang, Y., Saatchi, S. S., Xu, L., Yu, Y., Choi, S., Phillips, N., Kennedy, R., Keller, M., Knyazikhin, Y., & Myneni, R. B. (2018). Post-drought decline of the Amazon carbon sink. *Nature Communications*, *9*(1), 1–9. https://doi.org/10.1038/s41467-018-05668-6

Yazaki, K., Kuroda, K., Nakano, T., Kitao, M., Tobita, H., Ogasa, M. Y., & Ishida, A. (2015). Recovery of physiological traits in saplings of invasive Bischofia tree compared with three species native

to the Bonin Islands under successive drought and irrigation cycles. *PLoS One*, *10*(8), e0135117. https://doi.org/10.1371/journal.pone.0135117

Yee, T. W., & Mitchell, N. D. (1991). Generalized additive models in plant ecology. *Journal of Vegetation Science*, *2*(5), 587–602. https://doi.org/10.2307/3236170

Yuan, W., Zheng, Y. I., Piao, S., Ciais, P., Lombardozzi, D., Wang, Y., Ryu, Y., Chen, G., Dong, W., Hu, Z., Jain, A. K., Jiang, C., Kato, E., Li, S., Lienert, S., Liu, S., Nabel, J. E. M. S., Qin, Z., Quine, T., … Yang, S. (2019). Increased atmospheric vapor pressure deficit reduces global vegetation growth. *Science Advances*, *5*(8), eaax1396. https://doi.org/10.1126/sciadv.aax1396

Zeppel, M. J., Anderegg, W. R., & Adams, H. D. (2013). Forest mortality due to drought: Latest insights, evidence and unresolved questions on physiological pathways and consequences of tree death. *New Phytologist*, *197*(2), 372–374. https://doi.org/10.1111/nph.12090

Zhang, Y., Zhou, S., Gentine, P., & Xiao, X. (2019). Can vegetation optical depth reflect changes in leaf water potential during soil moisture dry-down events? *Remote Sensing of Environment*, *234*, 111451. https://doi.org/10.1016/j.rse.2019.111451

Zhao, M., & Running, S. W. (2010). Drought-induced reduction in global terrestrial net primary production from 2000 through 2009. *Science*, *329*(5994), 940–943. https://doi.org/10.1126/science.1192666

SUPPORTING INFORMATION

Additional supporting information may be found in the online version of the article at the publisher's website.

How to cite this article: Liu, L., Chen, X., Ciais, P., Yuan, W., Maignan, F., Wu, J., Piao, S., Wang, Y.-P., Wigneron, J.-P., Fan, L., Gentine, P., Yang, X., Gong, F., Liu, H., Wang, C., Tang, X., Yang, H., Ye, Q., He, B., … Su, Y. (2022). Tropical tall forests are more sensitive and vulnerable to drought than short forests. *Global Change Biology*, 28, 1583–1595. https://doi.org/10.1111/gcb.16017